ACS Photonics

Letter

pubs.acs.org/journal/apchd5

Design of Phosphor White Light Systems for High-Power Applications

Kristopher T. Bicanic,[†] Xiyan Li,[†] Randy P. Sabatini, Nadir Hossain, Cai-Feng Wang, Fengjia Fan, Hongyan Liang, Sjoerd Hoogland, and Edward H. Sargent*

Department of Electrical and Computer Engineering, University of Toronto, 10 King's College Road, Toronto, Ontario M5S 3G4, Canada

Supporting Information

ABSTRACT: We developed a strategy that transforms phosphor down-converting white light sources from low-power systems into efficient high-power ones. To incorporate multiple phosphors, we generalized and extended a phosphor layer model, which we term CCAMP (color correction analysis for multiple phosphors). CCAMP describes both the scattering and saturation of phosphor materials and allows modeling of different layered structures. We employed a phosphor mixture comprising YAG:Ce and $K_2TiF_6:Mn^{4+}$ to illustrate the effectiveness of the model. YAG:Ce's high density and small particle size produce a large amount of scattering, while the long (4.8 ms) photoluminescent lifetime of $K_2TiF_6:Mn^{4+}$ results in saturation at high pump power. By incorporating experimental photophysical results from the phosphors, we modeled our system and chose the design suitable for high-power applications. We report the first solid-state phosphor system that creates warm white light emission at powers up to 5 kW/cm^2. Furthermore, at this high power, the system's emission achieves the digital cinema initiative (DCI) requirements with a luminescence efficacy improvement of 20% over the stand-alone ceramic YAG:Ce phosphor.

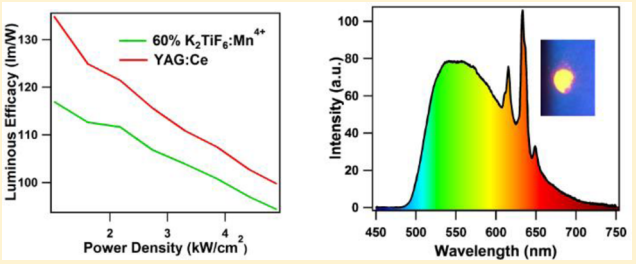

KEYWORDS: *phosphor, high-power light emission, white light source, red phosphor, YAG:Ce, $K_2TiF_6:Mn^{4+}$*

Since the late 2000s, traditional incandescent and fluorescent lighting have been increasingly supplanted by solid-state white light technology, which offers superior power efficiencies, low energy consumption, and long operation lifetime.[1,2] These benefits have led to applications in a wide range of areas, from low-power spot illuminators to high-power area illuminators.[3]

Two typical approaches exist when designing a white light emitting diode (LED), which requires red, green, and blue components. The first method combines individual red, green, and blue LEDs into a single package; however, this approach results in distorted color and incurs a high cost requirement associated with fabricating three LEDs.[2,4] Instead, the more widely practiced method incorporates down-converting phosphor materials that convert the output of a single source to lower energy light. This can be accomplished through an ultraviolet source, which excites three down-converters; or a blue light source, where a portion of its light is down-converted to red and green.[4] For applications involving high power densities (e.g., projection), the choice of phosphor is critical, as unfavorable photophysical properties can lead to precipitous drops in efficiency with increased power.

While the high-performing yellow-based $Y_3Al_5O_{12}:Ce^{3+}$ ($YAG:Ce^{3+}$) can operate efficiently at high radiances, this phosphor's spectrum prevents it from replicating a lower correlated color temperature (CCT).[1,5−11] The phosphor's emission spectrum can be corrected using two approaches: the first method filters out a portion of the green emission as waste (Figure 1b), whereas the preferred method introduces a secondary down-converter to increase the red emission, minimizing waste energy (Figure 1c).[12−15] Recently, Zhu et al. successfully demonstrated $K_2TiF_6:Mn^{4+}$ as a secondary down-converter for YAG:Ce; however, high flux illumination, necessary for high-power applications such as projection, was not reported.[16] While $K_2TiF_6Mn^{4+}$ has many advantageous properties,[16−22] it also possesses a ∼5 ms excited-state lifetime,[23] which results in saturation at high power, deleterious for efficiency.

The creation of a high-quality white light source can be accomplished with a multiphosphor system by designing an appropriate device architecture for high-power operation. It was demonstrated previously that a separate multilayered phosphor structure provided the highest performance;[24] however, there is a strong dependence on the phosphor materials used, device architecture, quantum efficiencies, and densities of the phosphor materials that need to be considered in the design.[25] To realize a high-power source, both scattering and saturation also need to be incorporated into the design protocol.

In this work, we develop a design strategy, enabled by the color-corrected analysis of multiple phosphors (CCAMP), to

Received: September 8, 2016
Published: November 16, 2016

DOI: 10.1021/acsphotonics.6b00681
ACS Photonics XXXX, XXX, XXX−XXX

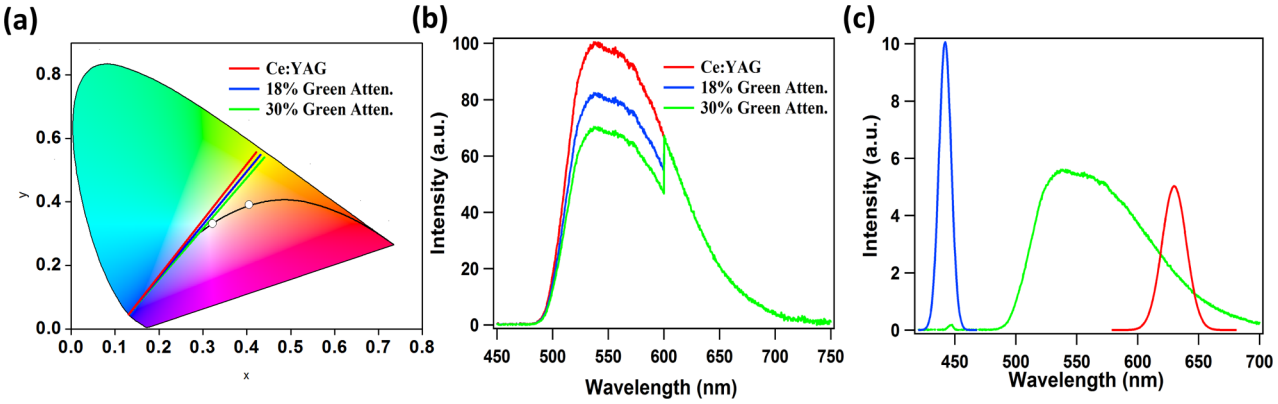

Figure 1. State-of-the-art YAG:Ce phosphor emission profiles and methods of color correction. (a) CIE color coordinates of YAG:Ce compared to standard blackbody radiation sources (black line). (b and c) Spectrally balanced emissions by filtering and spectral re-engineering.

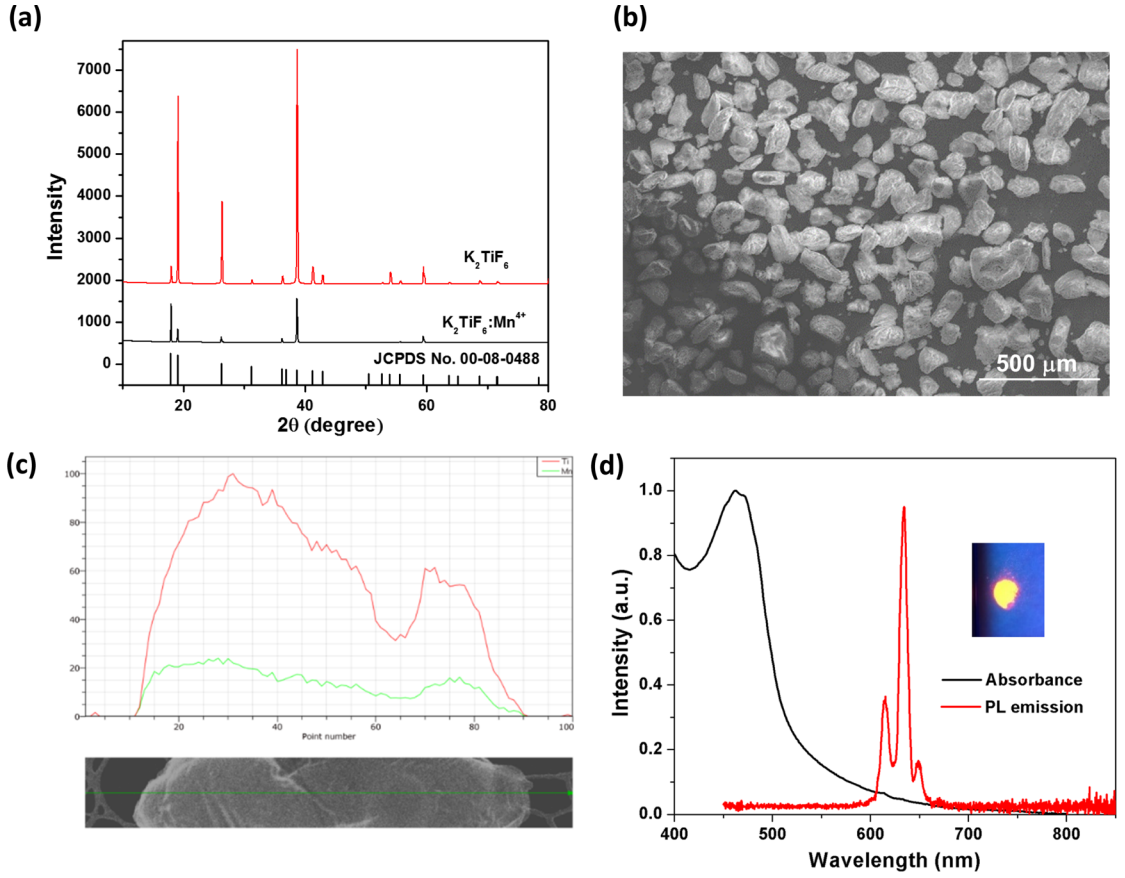

Figure 2. Structure and optical properties of K_2TiF_6:Mn^{4+} phosphors. (a) XRD data for K_2TiF_6 and K_2TiF_6:Mn^{4+} phosphor. (b) SEM image of K_2TiF_6:Mn^{4+} phosphor powder. (c) Elemental line scanning from a typical Mn^{4+}-doped K_2TiF_6 microparticle and SEM of analyzed cross section. (d) Absorption and PL emission of K_2TiF_6:Mn^{4+} phosphors. The inset shows photographs of the K_2TiF_6:Mn^{4+} sample under UV lamp illumination.

maintain the benefits of the high-efficiency YAG:Ce while spectrally engineering the emission through incorporation of red-emitting $K_2TiF_6Mn^{4+}$. This enables superior color for high-power white light sources. Using the CCAMP design model, we created a phosphor architecture to split the power between the high-performance phosphor and the red-emitting phosphor. We were therefore able to compensate for the saturation effects present in the $K_2TiF_6Mn^{4+}$ and scattering effects induced by the high loading of YAG:Ce, thereby achieving record performance for high-power (5 kW/cm^2) applications.

RESULTS AND DISCUSSION

The red emitter K_2TiF_6:Mn^{4+} was synthesized as in previous reports.[16,26] Pure K_2TiF_6 and Mn^{4+}-doped powders were characterized by XRD measurements (Figure 2a): diffraction peaks of the two samples can be indexed to tetragonal-phase K_2TiF_6 (JCPDS No. 00-008-0488). The particle size of the phosphors from SEM images (Figure 2b) ranges from 30 to 500 μm and shows a wide size distribution. Elemental line scanning for a typical Mn^{4+}-doped K_2TiF_6 microparticle shows a similar distribution between manganese and titanium along the cross section (Figure 2c). This is in agreement with

DOI: 10.1021/acsphotonics.6b00681
ACS Photonics XXXX, XXX, XXX−XXX

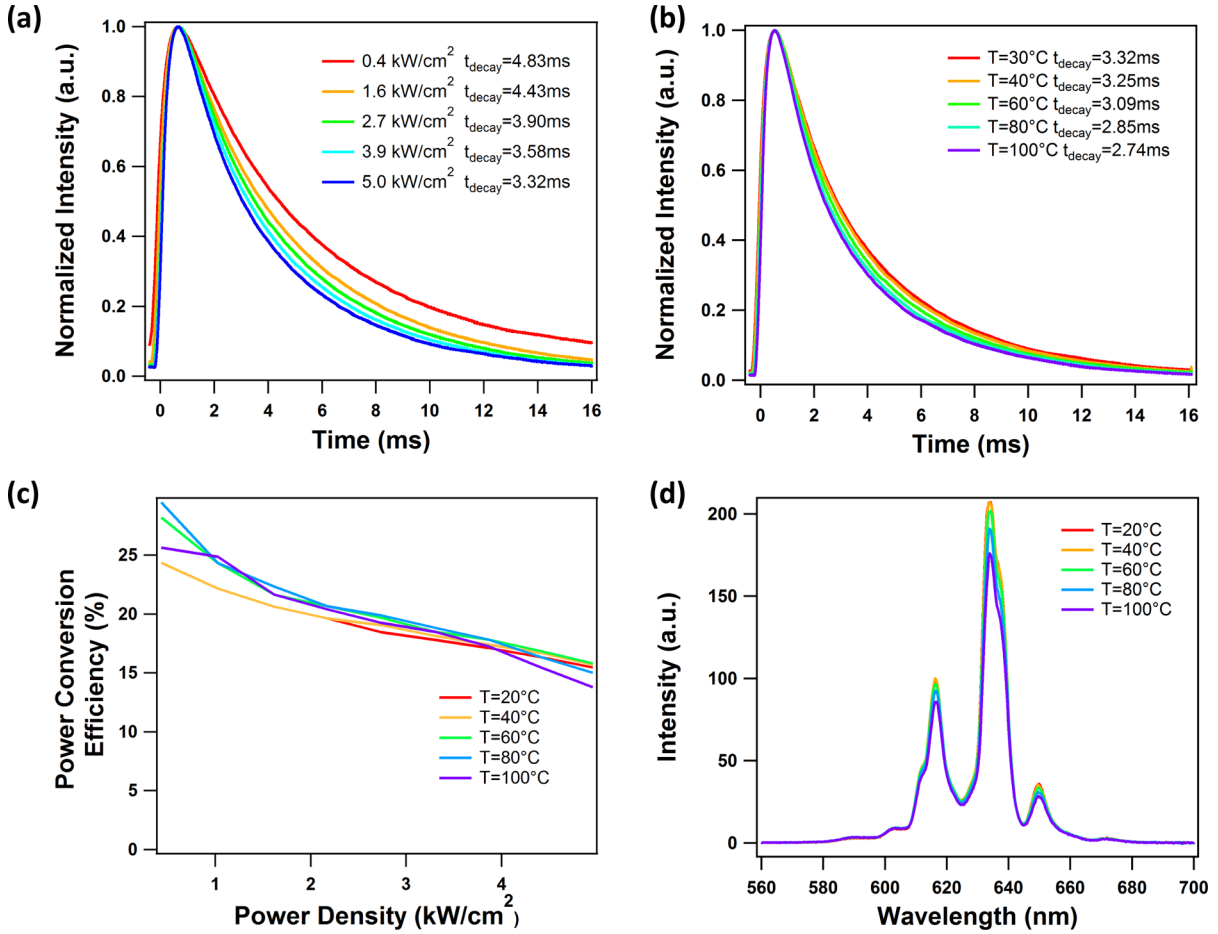

Figure 3. Emission characterization of K_2TiF_6:Mn^{4+} phosphors at high-power and high-temperature environment. (a) Photoluminescence lifetime dependence on power density. (b) Photoluminescence lifetime dependence on temperature at 5 kW/cm^2. (c) Power conversion efficiency of K_2TiF_6:Mn^{4+} phosphor at varying temperature. (d) Emission spectra of K_2TiF_6:Mn^{4+} at varying temperatures at a power density of 5 kW/cm^2.

mapping measurements from scanning transmission electron microscopy (STEM, Figure S1). The molar ratio of manganese to titanium was estimated to be 10% based on the calibrated signal intensities of energy-dispersive spectroscopy. These results demonstrate Mn^{4+} ion doping in the K_2TiF_6 matrix with uniform distribution throughout the microparticles.

The intense absorption band of the K_2TiF_6:Mn^{4+} microparticles (Figure 2d), positioned at 468 nm, overlaps well with the emission of conventional blue diodes. The overlap between the absorption of K_2TiF_6:Mn^{4+} and emission of YAG:Ce is negligible, thereby avoiding the reabsorption problem that usually occurs between (oxy)nitride red phosphors and yellow (or green) phosphors.[27] The red emission of K_2TiF_6:Mn^{4+} (Figure 2d) comprises three sharp peaks, with the main peak positioned at 631.5 nm (fwhm: 10 nm), with PLQYs up to 95%, similar to literature values.[22,23] Their narrowband spectra and high PLQYs enable high efficiency and excellent color quality for white LEDs.[14]

The CCAMP design process considers the extent of both scattering and saturation, allowing for the design of a high-power illumination source. The relative scattering coefficients were obtained by measuring the transmission of the dense phosphor layers for a given thickness. To determine the cause and effect of saturation, the photoluminescence (PL) lifetime and efficiency of the red phosphor were investigated as a function of power (experimental methods can be found in the Supporting Information). From this information and incorporating the scattering effects of the dense phosphor layers, a 1D model was built to investigate a range of phosphor architectures. Once the best architecture was obtained, we carried out a study to determine the appropriate ratio of red and green phosphors to achieve the desired white temperature.

The PL lifetime of K_2TiF_6:Mn^{4+} was observed to be 4.8 ms; this can cause saturation as a result of nonradiative decays. Here we investigated the power- and temperature-dependent lifetime of K_2TiF_6:Mn^{4+} using 442 nm excitation. When we adjust the peak power density from 0.4 kW/cm^2 to 5 kW/cm^2, the PL lifetime decreases by 31%, from 4.8 ms to 3.3 ms (Figure 3a). At 5 kW/cm^2, it further decreases from 3.3 ms to 2.7 ms upon a temperature increase from room temperature to 100 °C (Figure 3b). The decrease in the PL lifetime for both high power density and high temperature indicate an enhancement of nonradiative processes, which are detrimental to high power density operation at elevated temperature.

To determine the effect of saturation on performance, we measured the power conversion efficiency (PCE) with varying power and temperature (Figure 3c). Each temperature condition shows a decrease in PCE with increasing power, which is attributed to nonradiative decay. However, no temperature-dependent loss of efficiency occurs until both the highest power (5 kW/cm^2) and temperature (100 °C) are reached. As a result, when the new phosphor is mixed with yellow phosphor, the temperature-induced saturation effect is expected to be negligible, as the power will be distributed

DOI: 10.1021/acsphotonics.6b00681
ACS Photonics XXXX, XXX, XXX−XXX

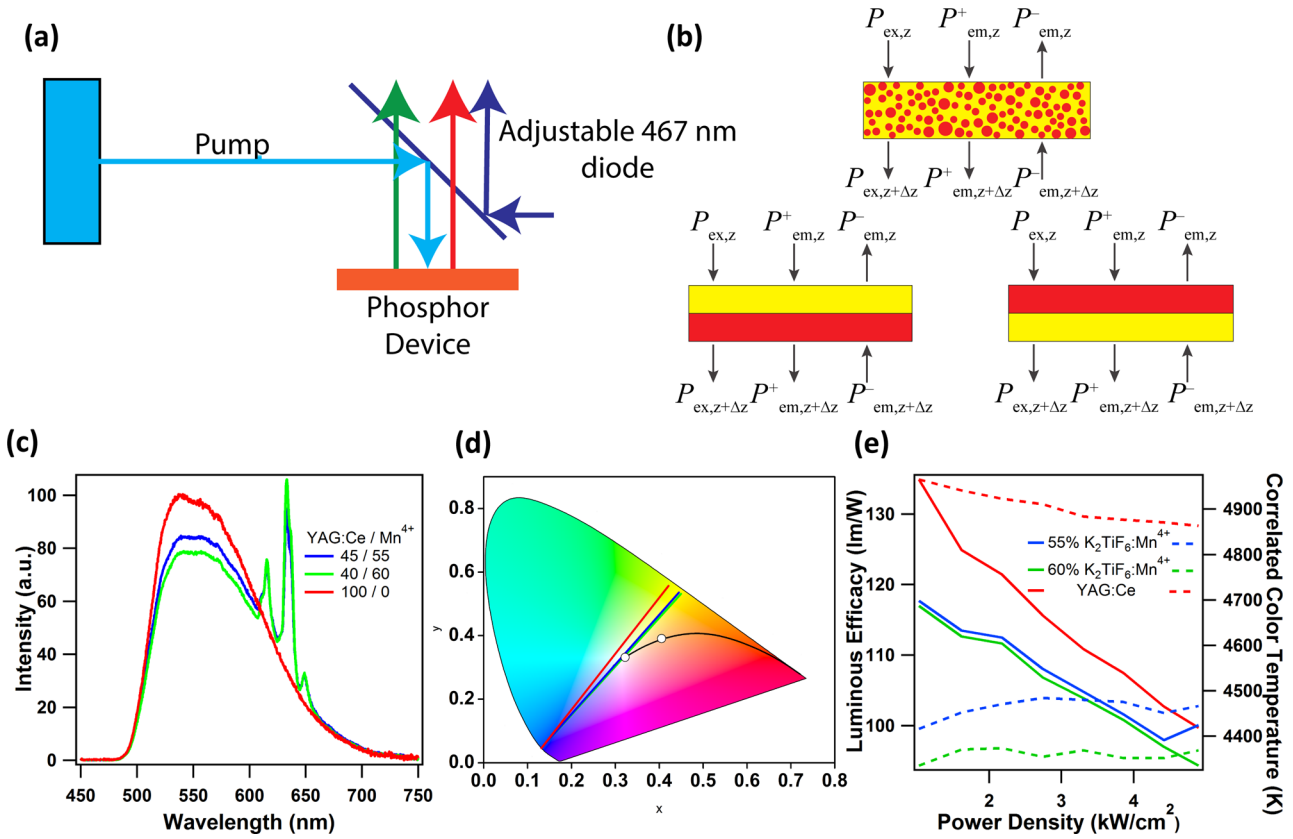

Figure 4. Engineering of a high-power, color-balanced white emitter based on the next-generation red phosphor. (a) Laser setup for excitation of phosphor and incorporation of blue source. (b) Test structures used to calculate red and yellow emission. (c) Spectrum of the YAG:Ce compared to the 55% and 60% $K_2TiF_6:Mn^{4+}$ structures. (d) CIE color coordinates of the samples at high flux excitation. (e) Luminous efficacy of two test samples and YAG:Ce with their respective CCTs.

between the red and yellow phosphors. Furthermore, the sample shows minimal loss in its emission at 5 kW/cm^2 until the highest temperatures are reached (Figure 3d).

To obtain white light emission, we designed a system that incorporated a pulsed blue excitation source used to excite down-converting phosphors YAG:Ce and $K_2TiF_6:Mn^{4+}$ (Figure 4a). The pulsed laser is used here to minimize saturation and thermal issues. Both phosphors were mixed into a silicone adhesive matrix (13% wt) to obtain a dense and smooth film, with a thickness less than 250 μm. The emission from the phosphors was efficiently transmitted through a dichroic mirror. For digital projection, this emission can be combined with an adjustable blue diode; for our analysis, we calculated the power required from a 467 nm source to produce the desired white color temperature (Figure 4a).

As part of the CCAMP process, we modeled various phosphor architectures, with the goal of operating as a solid-state lighting solution, as well as a source for high-power displays and projectors. Three different types of designs were adopted: layering the YAG:Ce phosphor on top and the $K_2TiF_6:Mn^{4+}$ phosphor as a base, the converse, and a homogeneous blend between the two materials (Figure 4b). We based our calculations on that provided by Kang[28] and extended it to incorporate the alternate architectures, as well as scattering and saturation. The model assumes a 1D transmission within the phosphor, using the following equations:

$$\frac{dP_{ex}}{dz} = -\alpha_{ex}P_{ex}(z) \tag{1}$$

$$\frac{dP_{em}^{+}}{dz} = -\alpha_{em}P_{em}(z) + \frac{1}{2}\alpha_{ex}\beta P_{ex}(z) \tag{2}$$

$$\frac{dP_{em}^{-}}{dz} = \alpha_{em}P_{em}(z) - \frac{1}{2}\alpha_{ex}\beta P_{ex}(z) \tag{3}$$

These three equations describe the intensity of light propagating within the phosphor materials. The first equation describes the power of the excitation source, P_{ex}. In this experiment, we used a 442 nm laser diode, focused to intensities up to 5 kW/cm^2. This equation accounts for absorption by the red- and green-emitting phosphors. The absorption of both phosphors is incorporated into the coefficient α_{ex} per unit length of the device, and thus α_{ex} depends on the phosphor composition in this layer. Equations 2 and 3 describe the emission of the red and yellow phosphors in the forward (2) and reverse (3) directions, respectively. Within these equations, α_{em} is the energy loss of the phosphor emission and β is the conversion efficiency of the excitation source to phosphor emission. This β term shows a power dependence based on the excitation power, which decreases as it is partially absorbed throughout the phosphor. The phosphor's emission power, $P_{em}^{\pm}$, was calculated for both red and yellow emission separately in the layered structures with $P_{em}^{\pm}$ phosphor emission traveling forward into the device and P_{em}^{-} emission traveling backward to the surface of the device. P_{em}^{-} at $z = 0$ is the collected emission, as the system architecture operates in reflection mode. As a mirror is located at the back of the device, $P_{em}^{-}(t) = P_{em}^{+}(t)$ at this position. The scattering of the excitation from the rear phosphor was calculated based on

DOI: 10.1021/acsphotonics.6b00681
ACS Photonics XXXX, XXX, XXX−XXX

the transmission properties of the top layer; this scattering is more pronounced in our system due to the higher loading densities when compared to lower power phosphor systems. The absorption saturation was incorporated into the K_2TiF_6:Mn^{4+} phosphor by using a linear fit to the PCE measured in Figure 3c and is incorporated into the β term for the K_2TiF_6:Mn^{4+} phosphor only.

The results of the model (Table 1) show that when a red phosphor is used as a base, the scattering induced from the YAG:Ce phosphor coating significantly reduces the red collection. Alternatively, when the YAG:Ce is the base, the yellow collection suffers due to the scattering in the K_2TiF_6:Mn^{4+} layer, and saturation of K_2TiF_6:Mn^{4+} limits the red emission. The homogeneous mixture, however, distributes the absorption and scattering losses throughout the entire device structure. This allows for the best balance between red and green power efficiency, which is a result of reduced red saturation.

Table 1. Model Tesults for K_2TiF_6:Mn^{4+} and YAG:Ce Phosphor Structures[a]

	mixture	red coating/yellow base	yellow coating/red base
green emission	25%	18%	44%
red emission	22%	39%	16%
total converted power output	47%	57%	60%
color-corrected power output	44%	31%	38%

[a]Excitation power converted to green and red emission shown. Desired color corrected power ratio of 55% green to 45% red emission.

As the coating layer's scattering has a detrimental effect on the lower layer, we chose to design the high-power devices using the red and yellow phosphor mixture. This allows us to distribute equally the scattering of both phosphors along the length of the device and not place the K_2TiF_6:Mn^{4+} under intense illumination, avoiding saturation. The highest performing devices were composed of 55% and 60% K_2TiF_6:Mn^{4+} by weight. The spectra of these samples (Figure 4c) were used to calculate the color coordinates of the phosphor mixtures with different red K_2TiF_6:Mn^{4+} concentrations at 5 kW/cm^2 (Figure 4d), in addition to the color temperature (Figure 4e).

Increasing the concentration of red phosphor raises the saturation threshold, thereby increasing the overall red-emitted power and by extension the balanced external quantum efficiency. At K_2TiF_6:Mn^{4+} concentrations of 55% and 60%, the yellow phosphor still absorbs sufficient light to maintain its performance at high power densities. This allows for high external efficiency, while also allowing the red emission to be increased, thereby correcting the spectrum (Figure 4d). CCT analysis of the spectra indicate minimal fluctuation in the color temperature for the 60% K_2TiF_6:Mn^{4+} phosphor mixtures at low and high power, ranging from 4335 to 4368 K, respectively (Figure 4d intercept with Planckian locus). This implies that the effect of any saturation with K_2TiF_6:Mn^{4+} is insignificant in this mixed system, as the effective pump power was decreased by the absorption of the yellow phosphor. Due to the invariance in color emission, the device structure successfully alters the YAG:Ce white emission such that it more closely approximates that of a warmer blackbody radiator. Furthermore, the phosphor mixtures exhibit high luminous efficacies, and thus high performance, at 5 kW/cm^2 (Figure 4e).

To operate the phosphor mixture as a source for displays, we must split the spectrum into green and red sources that meet the Digital Cinema Initiatives (DCI) color space standard's gamut. We introduced a 590 nm notch filter to separate the spectrum into green and red components, while removing a portion of the yellow emission. This allowed for the full gamut range required in digital projection. For the mixed systems of K_2TiF_6:Mn^{4+} and YAG:Ce, a balanced emission between red and green rendered the DCI white point with no waste energy. However, when separating the emission for the standalone YAG:Ce system, we remove a significant portion of the green emission to obtain the correct emission profile for the DCI white point. As a result, comparing to the mixture system, we achieved ~21% higher luminous efficacy when rendering white light, while also providing a wider gamut from the superior red source.

CONCLUSION

We established a design protocol, CCAMP, for analyzing device architectures with the goal of producing a highly efficient white light source. The effectiveness of this design protocol was demonstrated through the combination of an efficient YAG:Ce phosphor with a red-emitting K_2TiF_6:Mn^{4+} phosphor. The structure was shown to have superior performance for adjusting the temperature of white light at high fluxes. This allows the device, which would conventionally suffer from saturation and scattering of the red emitter, to exhibit improved color emission as a source for higher power applications. This mixed phosphor system, compared to standalone YAG:Ce at 5 kW/cm^2, provides a 21% luminescence improvement when used in cinematography, while for illumination it is capable of reducing the correlated color temperature to produce a warmer white light source.

ASSOCIATED CONTENT

Supporting Information

The Supporting Information is available free of charge on the ACS Publications website at DOI: 10.1021/acsphotonics.6b00681.

The experimental method for preparation of K_2TiF_6:Mn^{4+} phosphor powders, SEM imaging cross section of phosphor microparticles and elemental analysis, and energy-dispersive X-ray spectroscopy spectrum of K_2TiF_6:Mn^{4+} microparticles; photophysical experimental methods for power conversion efficiency and photoluminescence lifetime (PDF)

AUTHOR INFORMATION

Corresponding Author

*E-mail: ted.sargent@utoronto.ca.

ORCID

Kristopher T. Bicanic: 0000-0002-3020-4093

Author Contributions

[†]K. T. Bicanic and X. Li contributed equally to this work.

Notes

The authors declare no competing financial interest.

DOI: 10.1021/acsphotonics.6b00681
ACS Photonics XXXX, XXX, XXX−XXX

■ ACKNOWLEDGMENTS

This publication is based in part on work supported by the Natural Sciences and Engineering Research Council (NSERC) of Canada and the Ontario Centres of Excellence (OCE).

■ REFERENCES

(1) George, N. C.; Denault, K. A.; Seshadri, R. Phosphors for Solid-State White Lighting. *Annu. Rev. Mater. Res.* **2013**, *43*, 481−501.
(2) Shur, M. S.; Žukauskas, A. Solid-state lighting: Toward superior illumination. *Proc. IEEE* **2005**, *93*, 1691−1703.
(3) Tsao, J. Y.; Coltrin, M. E.; Crawford, M. H.; Simmons, J. A. Solid-State Lighting: An Integrated Human Factors, Technology, and Economic Perspective. *Proc. IEEE* **2010**, *98*, 1162−1179.
(4) Schubert, E. F.; Kim, J. K. Solid-state light sources getting smart. *Science* **2005**, *308*, 1274−1278.
(5) Schlotter, P.; Schmidt, R.; Schneider, J. Luminescence conversion of blue light emitting diodes. *Appl. Phys. A: Mater. Sci. Process.* **1997**, *64*, 417−418.
(6) Xie, R.-J.; Hirosaki, N.; Takeda, T. Wide color gamut backlight for liquid crystal displays using three-band phosphor-converted white light-emitting diodes. *Appl. Phys. Express* **2009**, *2*, 022401.
(7) Protesescu, L.; Yakunin, S.; Bodnarchuk, M. I.; Krieg, F.; Caputo, R.; Hendon, C. H.; Yang, R. X.; Walsh, A.; Kovalenko, M. V. Nanocrystals of cesium lead halide perovskites ($CsPbX_3$, X= Cl, Br, and I): novel optoelectronic materials showing bright emission with wide color gamut. *Nano Lett.* **2015**, *15*, 3692−3696.
(8) Meyer, J.; Tappe, F. Photoluminescent Materials for Solid-State Lighting: State of the Art and Future Challenges. *Adv. Opt. Mater.* **2015**, *3*, 424−430.
(9) Cantore, M.; Pfaff, N.; Farrell, R. M.; Speck, J. S.; Nakamura, S.; DenBaars, S. P. High luminous flux from single crystal phosphor-converted laser-based white lighting system. *Opt. Express* **2016**, *24*, A215−A221.
(10) Hu, C.; Shi, Y.; Feng, X.; Pan, Y. YAG:Ce/(Gd,Y)AG:Ce dual-layered composite structure ceramic phosphors designed for bright white light-emitting diodes with various CCT. *Opt. Express* **2015**, *23*, 18243−18255.
(11) Park, H. K.; Oh, J. R.; Do, Y. R. 2D SiNx photonic crystal coated $Y_3Al_5O_{12}:Ce^{3+}$ ceramic plate phosphor for high-power white light-emitting diodes. *Opt. Express* **2011**, *19*, 25593−25601.
(12) Sakuma, K.; Omichi, K.; Kimura, N.; Ohashi, M.; Tanaka, D.; Hirosaki, N.; Yamamoto, Y.; Xie, R.-J.; Suehiro, T. Warm-white light-emitting diode with yellowish orange SiAlON ceramic phosphor. *Opt. Lett.* **2004**, *29*, 2001−2003.
(13) Nersisyan, H.; Won, H. I.; Won, C. W. Highly effective synthesis and photoluminescence of $Sr_2Si_5N_8:Eu_{2+}$ red-emitting phosphor for LEDs. *Chem. Commun.* **2011**, *47*, 11897−11899.
(14) Pust, P.; Weiler, V.; Hecht, C.; Tücks, A.; Wochnik, A. S.; Henß, A.-K.; Wiechert, D.; Scheu, C.; Schmidt, P. J.; Schnick, W. Narrow-band red-emitting $Sr[LiAl_3N_4]:Eu^{2+}$ as a next-generation LED-phosphor material. *Nat. Mater.* **2014**, *13*, 891−896.
(15) Brinkley, S. E.; Pfaff, N.; Denault, K. A.; Zhang, Z.; Hintzen, H. T.; Seshadri, R.; Nakamura, S.; DenBaars, S. P. Robust thermal performance of $Sr_2Si_5N_8:Eu^{2+}$: An efficient red emitting phosphor for light emitting diode based white lighting. *Appl. Phys. Lett.* **2011**, *99*, 241106.
(16) Zhu, H.; Lin, C. C.; Luo, W.; Shu, S.; Liu, Z.; Liu, Y.; Kong, J.; Ma, E.; Cao, Y.; Liu, R.-S.; Chen, X. Highly efficient non-rare-earth red emitting phosphor for warm white light-emitting diodes. *Nat. Commun.***2014**, *5*.10.1038/ncomms5312
(17) Nguyen, H.-D.; Lin, C. C.; Fang, M.-H.; Liu, R.-S. Synthesis of $Na_2SiF_6:Mn^{4+}$ red phosphors for white LED applications by co-precipitation. *J. Mater. Chem. C* **2014**, *2*, 10268−10272.
(18) Wang, B.; Lin, H.; Xu, J.; Chen, H.; Wang, Y. $CaMg_2Al_{16}O_{27}:Mn^{4+}$-based Red Phosphor: A Potential Color Converter for High-Powered Warm W-LED. *ACS Appl. Mater. Interfaces* **2014**, *6*, 22905−22913.
(19) Sekiguchi, D.; Nara, J.-i.; Adachi, S. Photoluminescence and Raman scattering spectroscopies of BaSiF6:Mn4+ red phosphor. *J. Appl. Phys.* **2013**, *113*, 183516.
(20) Peng, M.; Yin, X.; Tanner, P. A.; Liang, C.; Li, P.; Zhang, Q.; Qiu, J. Orderly-Layered Tetravalent Manganese-Doped Strontium Aluminate $Sr_4Al_{14}O_{25}:Mn^{4+}$: An Efficient Red Phosphor for Warm White Light Emitting Diodes. *J. Am. Ceram. Soc.* **2013**, *96*, 2870−2876.
(21) Murphy, J. E.; Garcia-Santamaria, F.; Setlur, A. A.; Sista, S. 62.4: PFS, $K_2SiF_6:Mn^{4+}$: the Red-line Emitting LED Phosphor behind GE's TriGain Technology Platform. *Dig. Tech. Pap. - Soc. Inf. Disp. Int. Symp.* **2015**, *46*, 927−930.
(22) Sijbom, H. F.; Joos, J. J.; Martin, L. I. D. J.; Van den Eeckhout, K.; Poelman, D.; Smet, P. F. Luminescent Behavior of the $K_2SiF_6:Mn^{4+}$ Red Phosphor at High Fluxes and at the Microscopic Level. *ECS J. Solid State Sci. Technol.* **2016**, *5*, R3040−R3048.
(23) Lin, C. C.; Meijerink, A.; Liu, R.-S. Critical Red Components for Next-Generation White LEDs. *J. Phys. Chem. Lett.* **2016**, *7*, 495−503.
(24) Yiting, Z.; Nadarajah, N. Investigation of Remote-Phosphor White Light-Emitting Diodes with Multi-Phosphor Layers. *Jpn. J. Appl. Phys.* **2010**, *49*, 100203.
(25) You, J. P.; Tran, N. T.; Shi, F. G. Light extraction enhanced white light-emitting diodes with multi-layered phosphor configuration. *Opt. Express* **2010**, *18*, 5055−5060.
(26) Bode, H.; Jenssen, H.; Bandte, F. Über eine neue Darstellung des Kalium-hexafluoromanganats(IV). *Angew. Chem.* **1953**, *65*, 304−304.
(27) Piquette, A. P.; Hannah, M. E.; Mishra, K. C. An investigation of self-absorption and corresponding spectral shift in phosphors. *ECS Trans.* **2011**, *41*, 1−9.
(28) Kang, D. Y.; Wu, E.; Wang, D. M., Modeling white light-emitting diodes with phosphor layers. *Appl. Phys. Lett.***2006**, *89*.23110210.1063/1.2400111

DOI: 10.1021/acsphotonics.6b00681
ACS Photonics XXXX, XXX, XXX−XXX